Hindawi
Indoor Air
Volume 2024, Article ID 8834373, 13 pages
https://doi.org/10.1155/2024/8834373

Research Article

Effects of Window Position and Exhaust Flow Rate on Residential Kitchen Hood Performance: A Validated Numerical Approach

Yi-An Lin,[1] Ying-Chieh Chan,[2] and Wan-Chen Lee[1,3]

[1]*Institute of Environment and Occupational Health Sciences, National Taiwan University, Taipei, Taiwan*
[2]*Department of Civil Engineering, National Taiwan University, Taipei, Taiwan*
[3]*Global Health Program, National Taiwan University, Taipei, Taiwan*

Correspondence should be addressed to Wan-Chen Lee; wanchenlee@ntu.edu.tw

Received 16 August 2023; Revised 3 March 2024; Accepted 11 March 2024; Published 17 April 2024

Academic Editor: Faming Wang

Previous studies showed that opening windows could help with kitchen ventilation in pollutant removal. However, no studies have systematically examined the impacts of window positions on kitchen hood performance, and there is insufficient information on indoor airflow characteristics and pollutant distribution from makeup air through open windows. Therefore, the objective of this study was to use a validated computational fluid dynamics approach with CO_2 as an indoor air quality indicator (a surrogate for cooking emissions) to understand the impacts of exhaust flow rate and the window opening position on the flow characteristics, concentration distribution, and capture efficiency (CE) of the hood. We conducted four-point validation tests of the numerical models based on CO_2 concentration and temperature measurements under steady-state conditions. The validated models were subsequently used in simulations to understand the effects of six different window opening positions and the two exhaust flow rates on exposure. We found that the CO_2 concentration could be better reduced by having windows open at the higher location. Generally, the front windows were more effective with CE > 80%, followed by the back and the side windows, respectively. We also found that as the exhaust flow rate increased from 6.72 to 12.16 m^3/min, CE reached >75% for all window positions, where the most significant increase was 1.58 times for the lower side window. To sum up, changing the relative position of the window and the exhaust hood could help disperse the incoming airflow from the window, improve the kitchen's overall ventilation, and reduce pollutant concentration.

1. Introduction

Establishing a healthy indoor environment is essential because people spend most of their time indoors [1]. However, pollution from both indoor and outdoor sources has been linked to worsening indoor air quality (IAQ) and could pose various threats to human health [2]. Cooking activities were found to be a significant source of indoor pollution and could generate harmful substances such as particulate matter (PM), polycyclic aromatic hydrocarbons (PAHs), volatile organic compounds (VOCs), and other gaseous pollutants such as nitrogen dioxide (NO_2) and carbon dioxide (CO_2) [3–5]. For example, Ko et al. investigated the contributing factors of lung cancer in nonsmoking women in Taiwan and found that the risk was associated with an increased number of meals cooked per day [6]. Belanger et al. discovered that asthmatic children living in homes using gas stoves were more likely to have onsets of respiratory symptoms, and the association increased with rising indoor NO_2 concentration [7]. In another study by Hu et al., a decline in indoor NO_2 emissions was linked to a decreased incidence rate of pediatric asthma [8]. To reduce the concentration of cooking emissions and protect residents' health, the use of a kitchen exhaust hood could be an effective intervention strategy [9, 10]. Kitchen hood performance has been characterized in experimental studies. Factors such as hood flow rates, burner positions, and hood geometry designs were found to have considerable impacts on the hood performance [11–16]. However, these studies relied on measurements of cooking emissions at specific locations, and

information on the indoor flow characteristics and how they influence the pollutant distribution in the kitchen was limited.

The computational fluid dynamics (CFD) approach has been widely used in IAQ studies to supplement findings from experimental studies through modeling and simulation. Compared to full-scale experiments, a validated CFD approach could be more cost-effective and provide additional information, including continuous spatial distributions of the flow field, temperature, and target air pollutants through visualization. This information could further assist in understanding the exposure pathway of air pollutants, which provides insight into improving hood performance and reducing human exposure. Several studies have used the CFD approach to simulate the flow characteristics in the kitchen environment under various hood and environmental settings. For example, Zhou and Kim simulated the spatial distribution of CO_2 concentration and temperature in a residential open kitchen during cooking periods [17]. The results illustrated a better removal effect on CO_2 concentration and heat when the angle between the air inlet and ceiling decreased and under the higher flow rate (16.67 m^3/min). Zhou et al. investigated a new ventilation control system with the air curtain inlets surrounding the gas stove and the exhaust hood installed above in a residential kitchen [18]. The study demonstrated that the cooking emissions and the thermal environment could be well controlled and improved with the air curtain system. Chen et al. analyzed the distribution of PM-based cooking emissions and the thermal condition under different flow rates of the exhaust hood by using a validated kitchen environment simulation model. The optimal condition was achieved as the exhaust flow rate increased above 11 m^3/min [19]. Le Hocine et al. assessed the impacts of the number of in-use burners and flow rate by modeling the exhaust hood performance in a residential kitchen [20]. They used CO_2 as the tracer gas and found that the capture efficiency (CE) was 100% when the flow rate reached 8.5 m^3/min. Yi et al. employed a concurrent supply and exhaust ventilation system in the kitchen and effectively improved the hood performance with the optimum flow rate of 1.6 m^3/min [21]. In essence, most studies indicated that an increase in the hood flow rate or using an additional supply air system helped with air pollutants and heat removal. However, the former approach could also lead to excessive energy consumption and noise [22]. Therefore, setting the flow rate at a range that ensures effective pollutant removal while minimizing the undesirable effects is crucial.

The use of a kitchen hood could influence indoor ventilation in two ways: by providing local air exhaust in the proximity of the cooking area and general ventilation in the household with the introduction of ambient makeup air. For Chinese-style residential kitchens, ventilation using natural makeup air from window openings or cracks consisted of prevalent scenarios [23, 24]. However, very few studies have evaluated the influence of ventilation conditions on hood performance. Sun and Wallace investigated 132 Canadian homes and pointed out that exposure to cooking emissions could be well reduced with the window openings in the kitchen [25]. Wang et al. modeled the flow characteristics in the residential kitchen under nine scenarios with a combination of an open window and/or door under different exhaust flow rates [26]. The results showed that only opening the window would considerably improve IAQ around the cooking zone under the same flow rate, and the window location could be an influential factor. He et al. studied the effects of natural makeup air on hood performance by measuring time-elapsed particle concentrations during oil heating experiments in a simulated Chinese residential kitchen [27]. They set up five different openings (three window openings on the same side, a ceiling-mounted opening, and a floor-mounted opening) and found substantial leakage when opening the window closest to the stove. The authors concluded that the leakage could be alleviated by adjusting the window position or supplying makeup air through the mounted openings. In their study, the effects of the window's spatial orientation and CE quantification remained unidentified.

Although opening windows could help with kitchen ventilation in pollutant removal, no studies have systematically examined the impacts of window positions on hood performance. Furthermore, there is insufficient information on indoor airflow characteristics and pollutant distribution from makeup air through open windows. Therefore, the objective of this study was to use a validated CFD approach with CO_2 as an IAQ indicator (a surrogate for cooking emissions) to understand the impacts of exhaust flow rate and the window opening position on the flow characteristics, concentration distribution, and CE of the hood. A total of 12 scenarios (six window positions and two flow rates) were evaluated.

2. Materials and Methods

2.1. Study Zone. The experimental study was conducted in the laboratory where the dimensions of the study zone were 3.9 m in length, 3.1 m in width, and 3.6 m in height. Figure 1 shows the reconstructed schematic diagram of the study zone for the CFD simulation. The minor physical structures, such as pipes and cables, were simplified in the three-dimensional (3D) model for a more efficient computing process. A cooking station with an artificial pollutant generation system and a kitchen exhaust hood was set up to simulate hood operation during cooking activities. We used a heating chamber to provide a buoyant plume and a round opening on the top to approximate the cooking condition with a 28 cm diameter pan heated on an electric stove. Constant CO_2 emission from the gas cylinder was directed into the heating chamber as a surrogate of gaseous pollutants through a duct equipped with a small mixing fan (8 cm × 8 cm). The chamber also contained particle emissions from the nebulizers at a constant rate; however, only CO_2 measurements are presented in this study. An exhaust hood with two vertical side panels was installed 70 cm away from the opening of the heating chamber and 1.65 m from the ground level. The side panels were expected to ensure high removal efficiency for the cooking emissions, consistent with a similar design suggested by Zhao et al. The authors employed a CFD

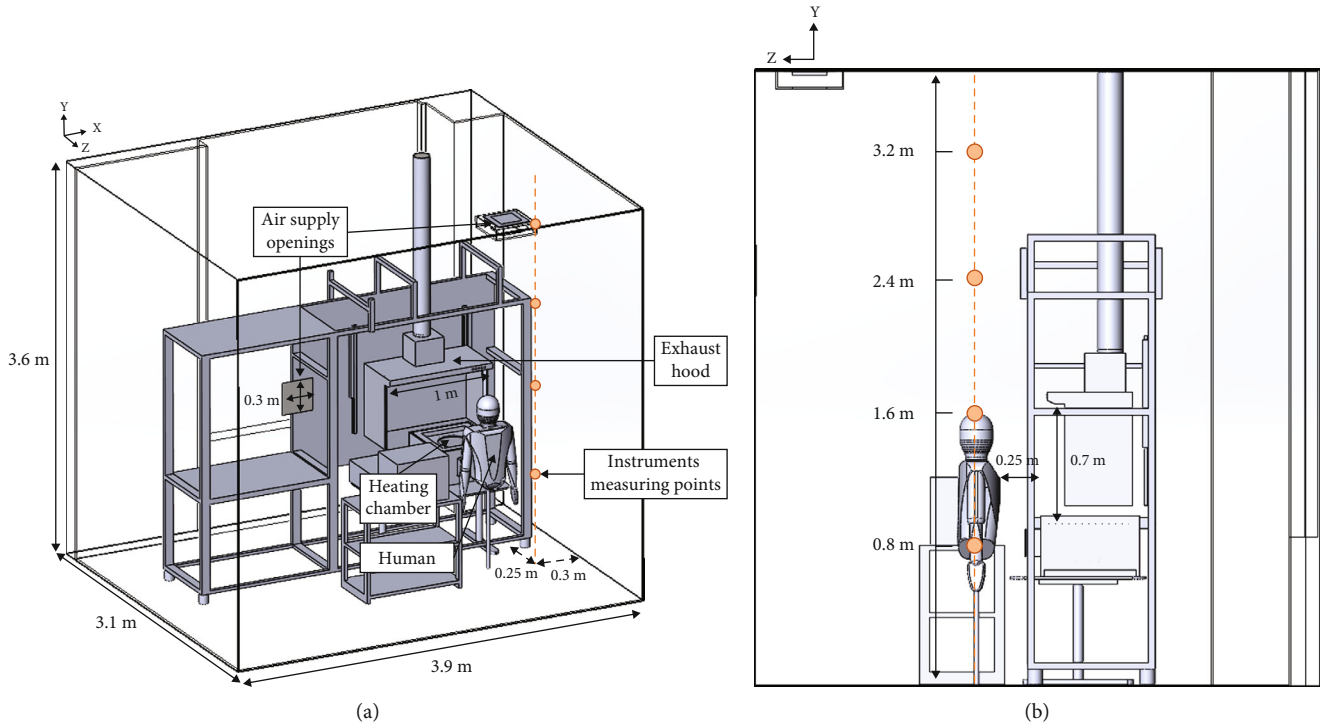

FIGURE 1: Schematic diagram of the simulated kitchen environment: (a) the full view and (b) the side view.

approach to evaluate the hood performance among 21 residential exhaust hoods with different geometric designs and found that the capture and containment efficiency could be enhanced by 20% with the installation of the side panels [28]. The dimensions of the hood were 100 cm in length, 50 cm in width, and 67 cm in height, with other detailed information described in the Supplemental Information (SI) (SI-1, Figure S1). Additionally, a 1.6 m tall human model was placed at a distance of 25 cm from the heating chamber to mimic the standing position of a person while cooking. The breathing zone was defined as a 30 cm radius from the nose of the human model, which was at the height of 1.5 m. Finally, there were two openings (30 cm × 30 cm) in the wall and the ceiling, respectively. Under the operation of the exhaust hood, the fresh, ambient air was passively introduced into the study zone through these openings.

2.2. Experimental Procedure. Experiments were carried out to validate the predicted numerical results based on the steady-state conditions of CO_2 concentration and temperature to ensure the reliability of the simulation in triplicate. In each experiment, we first started the constant CO_2 emission at the flow rate of 0.00036 m^3/min to introduce the pollutant into the heating chamber. The temperature of the coil in the heating chamber was set at 350°C to provide a buoyant plume to simulate that from cooking activities. We maintained the air exchange rate using the CO_2 constant injection method at 2 per hour by manually adjusting the openings of the study zone [29]. Detailed measurement procedure of air exchange rate can be found in SI (SI-2). Based on the mass balance model, the concentration of the artificial pollutant followed an exponential increase and eventually reached the steady state, where the CO_2 concentration and the temperature in the breathing zone of the human model were maintained at 3000 ppm and 32°C, respectively. We subsequently turned on the exhaust hood flow rate from low (6.72 m^3/min) to high (12.16 m^3/min) and waited for the CO_2 concentration to reach the new steady states under the hood operation. We then measured the CO_2 concentrations and the temperature concurrently at four vertically aligned locations ($Y = 0.8$ m, 1.6 m, 2.4 m, and 3.2 m) on the right side of the human model (Figure 1), in conjunction with one measurement point outside of the study zone to monitor the ambient environmental condition. All instruments were calibrated, and their detailed information is listed in SI (SI-3, Table S1). The three repeated measurements from the four vertical locations were then used for the validation tests with the simulation results.

2.3. Numerical Method. The 3D computational model in the study was implemented in SolidWorks Flow Simulation [30]. The steady-state flow field in SolidWorks was solved based on the Favre-averaged Navier-Stokes equations, together with the modified $k-\varepsilon$ turbulence model to close the equations. The Favre-averaged Navier-Stokes equations consist of the continuity, momentum, and energy equations, respectively (Equations (1)–(3)). They are defined as follows:

$$\frac{\partial \rho}{\partial t} + \frac{\partial (\rho u_i)}{\partial x_i} = 0, \tag{1}$$

$$\frac{\partial (\rho u_i)}{\partial t} + \frac{\partial (\rho u_i u_j)}{\partial x_j} + \frac{\partial p}{\partial x_i} = \frac{\partial}{\partial x_j}\left(\tau_{ij} + \tau_{ij}^R\right) + S_i, \tag{2}$$

$$\frac{\partial \rho H}{\partial t} + \frac{\partial \rho u_i H}{\partial x_i} = \frac{\partial}{\partial x_i}\left[u_j\left(\tau_{ij} + \tau_{ij}^R\right) + q_i\right] + \frac{\partial \rho}{\partial t} - \tau_{ij}^R \frac{\partial u_i}{\partial x_j} + \rho\varepsilon + S_i u_i + Q_H, \quad (3)$$

$$H = h + \frac{u^2}{2}, \quad (4)$$

$$\tau_{ij} = \mu\left(\frac{\partial u_i}{\partial x_j} + \frac{\partial u_j}{\partial x_i} - \frac{2}{3}\delta_{ij}\frac{\partial u_k}{\partial x_k}\right), \quad (5)$$

$$\tau_{ij}^R = \mu_t\left(\frac{\partial u_i}{\partial x_j} + \frac{\partial u_j}{\partial x_i} - \frac{2}{3}\delta_{ij}\frac{\partial u_k}{\partial x_k}\right) + \frac{2}{3}\rho k\delta_{ij}, \quad (6)$$

where ρ is the air density; u_i and u_j are the fluid velocity in x-, y-, and z-directions ($i, j = x$-, y-, z-directions); t is the time; p is the pressure; τ_{ij} is the viscous shear stress tensor (Equation (5)); τ_{ij}^R is the Reynolds stress tensor (Equation (6)); S_i is the external force; q_i is the diffusive heat flux; ε is the turbulence dissipation rate; Q_H is the internal heat generation; h is the thermal enthalpy; μ is the viscosity; δ_{ij} is the Kronecker delta function; k represents the turbulent kinetic energy; and μ_t is the eddy viscosity. Additionally, the $k-\varepsilon$ turbulence model proposed by Lam and Bremhorst was employed in the calculation [31]. Finally, to solve the complex algorithm, SolidWorks Flow Simulation used a pressure-based solver and SIMPLE algorithm to decouple the velocity and pressure to simulate the flow field [32].

2.3.1. Boundary Conditions. The boundary conditions were primarily based on the settings in the validation experiments and the ambient environmental conditions (Table 1). The wall materials were defined to account for the heat conduction in the laboratory environment. The initial condition inside the study zone for the CFD simulation was set to be 3000 ppm for the CO_2 concentration and 32°C for the temperature, representing the steady-state condition when the exhaust hood was turned off. The study zone was divided by the cube shape and Cartesian-based grids for the grid generation, where the local grids were refined around the window, the hood, and the heating chamber regions. The detailed grid size is defined in Section 2.3.2.

2.3.2. Model Validation. We conducted the grid independence test before the CFD simulation results were valid for analysis. Four mesh cases were tested per number of total grids. They were named mesh cases 1, 2, 3, and 4, comprising 7.8×10^5, 9.5×10^5, 1×10^6, and 1.07×10^6 grids, respectively. The simulation results of the optimal grid condition were subsequently compared with the averaged experimental results at the four measurement locations shown in Figure 1. The validation was considered acceptable if the calculated difference ratio (Equation (7)) between the simulation and experimental values was below 10% at each measurement location.

$$\text{Difference ratio}\,(\%) = \left|\frac{\text{experimental value} - \text{simulation value}}{\text{experimental value}}\right| \times 100\%. \quad (7)$$

2.4. Simulation Cases. We modified the validated baseline CFD model to simulate a more representative kitchen layout. The cooking station was repositioned against the wall, and the ceiling opening was removed, as shown in Figure 2. Additionally, we increased the size of the window to 0.3 m × 0.6 m in dimension. Six different window opening positions were selected, with two each on the front, side, and back orientation of the kitchen walls. The front side represents the wall where the human model was facing, whereas the back refers to the wall behind the human model. The side windows were installed in the wall on the right-hand side of the human model. Furthermore, considering the location of the transom openings commonly found in Taiwanese residences, we set the window positions at two different heights (1.2 and 2.4 m) at the same horizontal position of each wall. Information on the six window opening positions is summarized for the simulation cases in Table 2.

We presented the simulation results of the CO_2 concentration and the flow field across the breathing plane defined as the vertical plane cut from the center of the measurement point in the breathing zone (Figure 3). We also determined the CO_2-based CE using Equation (8) developed by Li and Delsante to characterize the hood performance for each simulation case under the steady-state conditions [33].

$$\text{CE}\,(\%) = \frac{\text{conc.in the exaust duct} - \text{conc.in the breathing zone}}{\text{conc.in the exaust duct} - \text{ambient conc.}} \times 100\%. \quad (8)$$

3. Results

3.1. Grid Independence Test and Model Validation. We compared the simulation results of the CO_2 concentration and temperature by the height of the measurement locations for the four mesh cases (Figure 4). As the grid number increased, the simulation values showed a similar trend in mesh cases 3 and 4. In Figure 4, the values at the height of 2.5-3 m were slightly different between mesh cases 3 and 4; however, the values at the other sampling points were in good agreement. Overall, the grid test was considered to have reached independence. Using the experimental results as the baseline values, the difference ratios for mesh cases 3 and 4 were under 10% at all measurement locations and were considered acceptable for validation (Table 3). Mesh case 3 was chosen for the follow-up simulation cases (Section 3.2) because it had better computational efficiency due to the lower number of grids than mesh case 4. As a result, mesh case 3 could reasonably reflect the spatial distribution of CO_2 concentration and temperature in the kitchen environment under hood operation.

3.2. Simulation Cases

3.2.1. Distribution of the Flow Field by Exhaust Flow Rate. We used mesh case 3 to simulate the cases for different

Table 1: Parameters and their values for the boundary conditions.

Boundary	Type	Flow parameter	Temperature	Air : CO_2 volume fraction
Hood outlet	Volume outlet	Low: 6.72 m^3/min High: 12.16 m^3/min	—	—
CO_2 inlet	Volume inlet	0.00036 m^3/min	26.5°C	0 : 1
Nebulizer inlet	Volume inlet	0.011 m^3/min	26.5°C	0.9996 : 0.0004
Mixture fan	Volume inlet/outlet	0.566 m^3/min	26.5°C —	0.9994 : 0.0006 —
Windows	Pressure openings	101325 Pa	26.5°C	0.9996 : 0.0004
Ceiling opening	Pressure openings	101325 Pa	26.5 °C	0.9996 : 0.0004
Boundary	Type	Materials		Temperature
Heating coil	Wall	Copper		350°C
Wall	Wall	Cast concrete		—
Heating chamber	Wall	AISI 304		—
System structure	Wall	Aluminum 6061		—
Exhaust hood	Wall	AISI 304		—
Human model	Wall	PVC		—

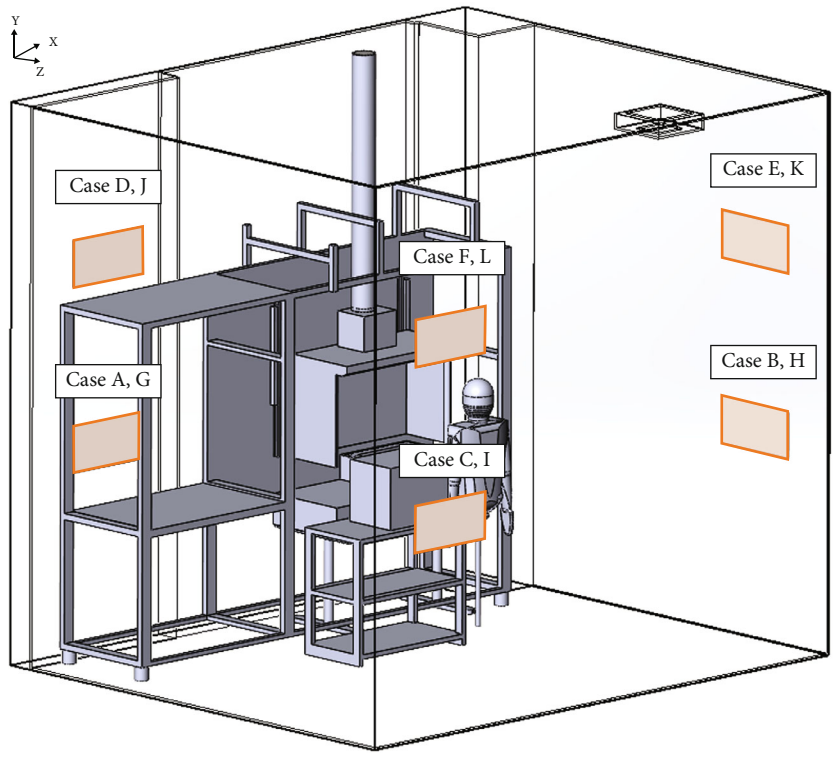

Figure 2: Window positions for each simulation case.

window opening locations, where the maximum and minimum grid sizes were 60 mm and 3.75 mm, respectively (Figure 5). Figure 6 shows the distribution of the CO_2 concentration at the steady state under the low (6.72 m^3/min) and high (12.16 m^3/min) flow rates for different window positions. When the exhaust hood flow rate was low, the hood demonstrated variable performance in removing the emitted CO_2, which was leaked from the proximity of the exhaust hood in all six cases. The leaked CO_2 accumulated in the upper space of the kitchen, following the vertical temperature gradient established by the buoyancy effect of the heat released from the simulated cooking activity (SI-4, Figure S2). When the exhaust flow rate increased to 12.16 m^3/min, the hood showed improved performance in removing the pollutants, leading to a decreased level of escaped CO_2. However, an accumulation of CO_2 was

Table 2: Parameters for the simulation cases.

Exhaust flow rate (m^3/min)	Window height (m)	Window position		
		Front	Side	Back
6.72	1.2	Case A	Case B	Case C
	2.4	Case D	Case E	Case F
12.16	1.2	Case G	Case H	Case I
	2.4	Case J	Case K	Case L

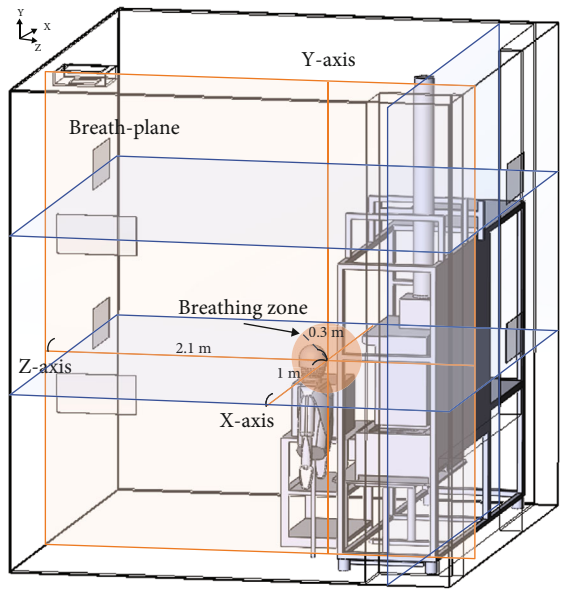

Figure 3: Diagram for the *y-z* plane at the measurement point of the breathing zone, *x-z* plane at the center of the window, and *x-y* plane at the center of the chamber.

observed in cases G, H, and L, suggesting that window positions could still be an influential factor in pollutant distribution under the high exhaust flow rate.

3.2.2. Distribution of the Flow Field by Window Height. For different window installation heights, CO_2 concentration gradients with varying degrees were observed for cases with a lower window position (cases A, B, and C). The concentrations were higher in the space above the exhaust opening of the hood, compared to those in cases D, E, and F (Figure 6(a)). To assess the extent of the concentration gradient, we compared the maximum and minimum CO_2 values from the *y-z* plane of the measurement points used in the previous validation tests. The concentration difference ranged from 310 to 1080 ppm for the cases with a lower window position. In contrast, it decreased by approximately 50% for the cases with a higher window position and ranged from 160 to 510 ppm, suggesting better air mixing. Figure 7(a) shows the CO_2 concentration and the airflow field under the low flow rate in the *x-z* plane from the center of the window and the *x-y* plane from the center of the heating chamber. As mentioned previously, there was a temperature gradient with higher CO_2 concentration near the ceiling due to the buoyancy effects from simulated cooking activities. When the cooler ambient air entered from the upper window, it went downwards and carried part of the CO_2 from the higher space to the bottom of the kitchen, which facilitated air mixing and the dilution of CO_2 concentration near the ceiling. On the other hand, when the window was placed at lower positions, the cooler ambient air had the tendency to stay at the bottom of the space. The results showed that exhaust hood performance was better in cases with windows located at the height of 2.4 m than 1.2 m.

3.2.3. Distribution of the Flow Field by Window-Wall Locations. In addition to the window height, the window-wall locations (front, side, and back) were found to influence pollutant removal by the kitchen hood, and the effect was more pronounced under the low flow rate (Figure 7). When the window was in the front wall (cases A and D), the CO_2 concentrations in the kitchen were lower than those in the back or side walls. We further used cases D, E, and F (the low flow rate and the high window position) as examples to discuss how the selection of the window-wall location affected the flow field inside the kitchen (Figure 8). For case D, as the fresh air entered from the upper front window, a counterclockwise vortex was generated in the kitchen. The vortex contributed to the pollutant removal in two aspects: (1) it enhanced the air mixing and (2) it carried the pollutant along the way to the hood at the end of the vortex and facilitated the pollutant exhaust. On the other hand, the flow field of case E showed that the fresh makeup air entered from the back window and flowed clockwise inside the kitchen, creating multiple vortexes as it reached the cooking station. The vortexes interfered with the pollutant capture at the hood, which subsequently led to the accumulation of CO_2 concentration in the kitchen. As for case F, the makeup air moved towards and reached the front wall. As the air turned and circulated in the kitchen, it disturbed the thermal plume around the cooking station, leading to CO_2 escape from the range of the hood and accumulation on the left side of the kitchen space.

3.2.4. CE of the Simulation Cases. We used CE as the hood performance metric to assess the impact of window position on CO_2 removal under the two flow rates (Table 4). In general, CE was higher when the windows were in the front wall, followed by the back and side walls. Exceptions were found for the cases with high window positions under the high flow rate (cases K and L). Under the low flow rate, CE ranged from 33 to 83%, with the lowest value for the low window position in the side wall (case B) and the highest for the high window position in the front wall (case D). On the other hand, CE increased by flow rate and ranged from 77 to 97%, depending on the window positions. The most significant impact was observed for the case with a low window position in the side wall, where a 1.8 times increase in flow rate (from low to high) resulted in a 1.58 times increase in CE.

4. Discussion

We found that the CO_2 concentration distribution and the hood performance were influenced by the window height,

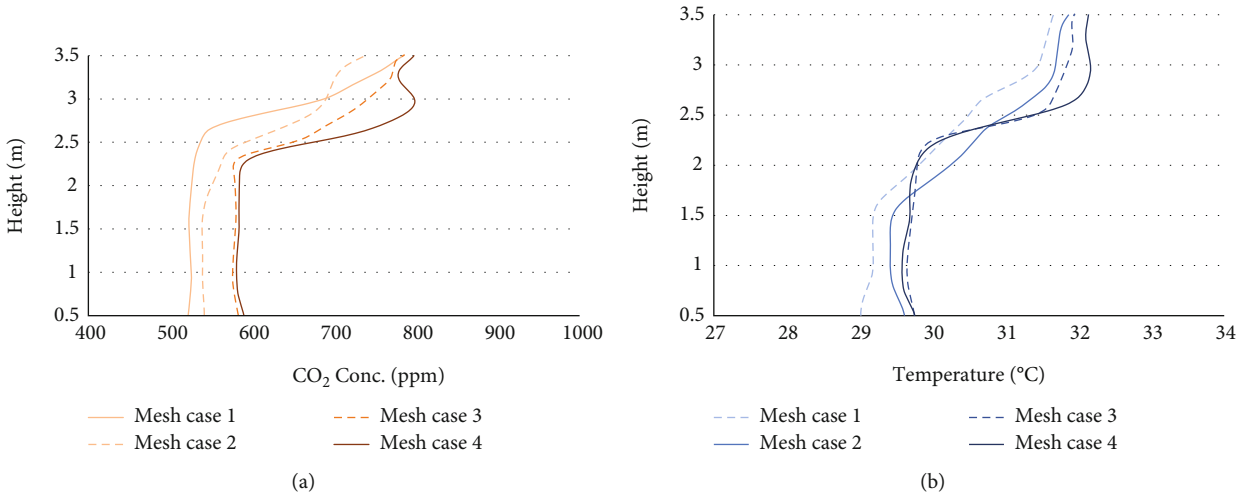

Figure 4: Comparison between simulation values of (a) CO_2 concentration and (b) temperature by the height of the measurement locations.

Table 3: The difference ratio of the CO_2 concentration and temperature at four measurement locations for the two mesh cases.

Height (m)	0.8	1.6	2.4	3.2
Difference ratio (%) of mesh case 3				
CO_2	4	7	10	7
Temp.	4	3	3	3
Difference ratio (%) of mesh case 4				
CO_2	3	6	7	9
Temp.	4	3	3	2

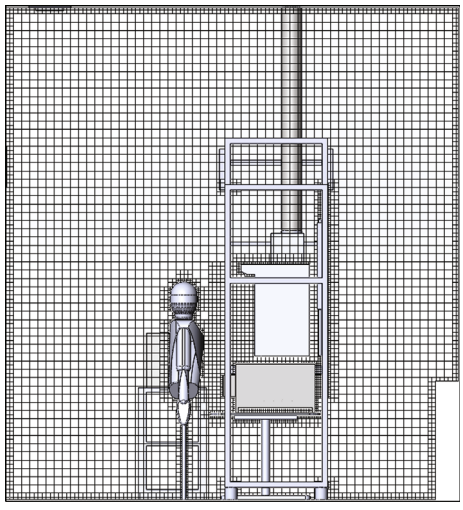

Figure 5: Side view of the grid distribution of mesh case 3.

the relative position between the window and the hood, and the exhaust flow rate. We based the discussion on comparisons to findings from previous studies and additional simulation results.

4.1. Distribution of CO_2 Concentration and CE by Window Height. We found that the exhaust hood generally performed better in removing CO_2 for cases with windows at the height of 2.4 m than 1.2 m. However, for the back window cases I and L under the high flow rate, higher CE was observed for using the lower window. This could be explained by the CO_2 leakage from the hood region due to the disturbance of buoyant plume by the high-velocity makeup air from the back window. For example, in case L, the contamination was pushed to the side of the hood, resulting in leakage (Figure 7(b)). When the rising thermal plume was disturbed by the makeup air, it would affect the capture area of the hood. Chen et al. examined the hood performance under the effects of the cross draft from lateral, oblique, and front directions [34]. They found that cross draft could lead to the spillage of cooking emissions, and the effect worsened as the airflow velocity increased. Similar findings were reported by Wang et al., who simulated the particle distribution under three different ventilation modes (only window open, only door open, and window and door open) with three different exhaust hood flow rates (5, 8.64, and 12.96 m^3/min) during cooking processes [26]. They found that the incoming air from the window or the door (located at each side of the human model) would interfere with the thermal plume and reduce the hood performance around the cooking area. To confirm the mechanism mentioned above, we conducted an additional analysis to decrease the influence of the cross airflow by modifying the kitchen space to two times larger than the original space. This approach led to an elongated route for the makeup air to reach the cooking station and thus reduced the velocity of the incoming air. The findings from the additional analysis were consistent with those from the other scenarios. Further details are included in SI (SI-5, Figure S3 and S4). In sum, we found that the relative position between the window and the exhaust hood could affect the hood performance.

It is noteworthy that the variable vertical concentration gradient under different flow and window settings had a relatively mild impact on CE because it was determined based on CO_2 concentration at the same location in the breathing zone. Additionally, the breathing zone was located in the middle region of the space and was less sensitive to the extreme values of the concentration gradient. As a result,

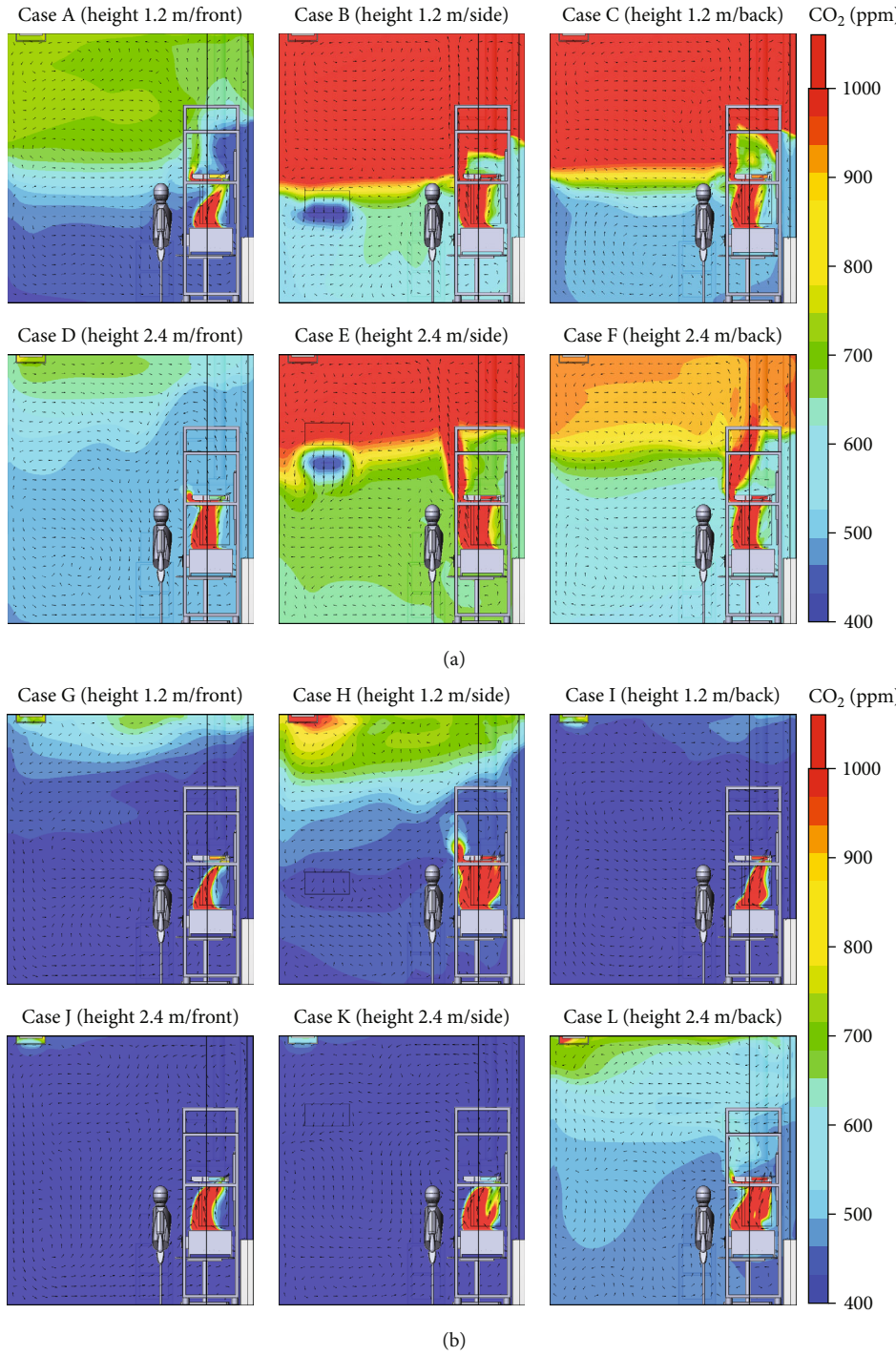

FIGURE 6: Distribution of the CO_2 concentration and the airflow velocity in the y-z plane in the breathing zone under the flow rate of (a) 6.72 m^3/min and (b) 12.16 m^3/min. The airflow velocity is presented using vectors, whereas the color contour describes the distribution of CO_2 concentration.

CE could be considered a more robust index for hood performance and suitable for cross-study comparisons.

4.2. Comparison of CE to Other Studies. In this study, we assessed the impacts of six different window locations on CO_2-based CE and found that the kitchen hood performed better under the high flow rate with the front, side, and upper back windows open. The performance decreased drastically when the flow rate decreased. The change in hood performance could be well explained by the presentation of the flow characteristics and the distribution of CO_2 concentration in the study zone from the simulation results.

CE has been widely applied in previous studies to investigate the influential factors for kitchen hood performance,

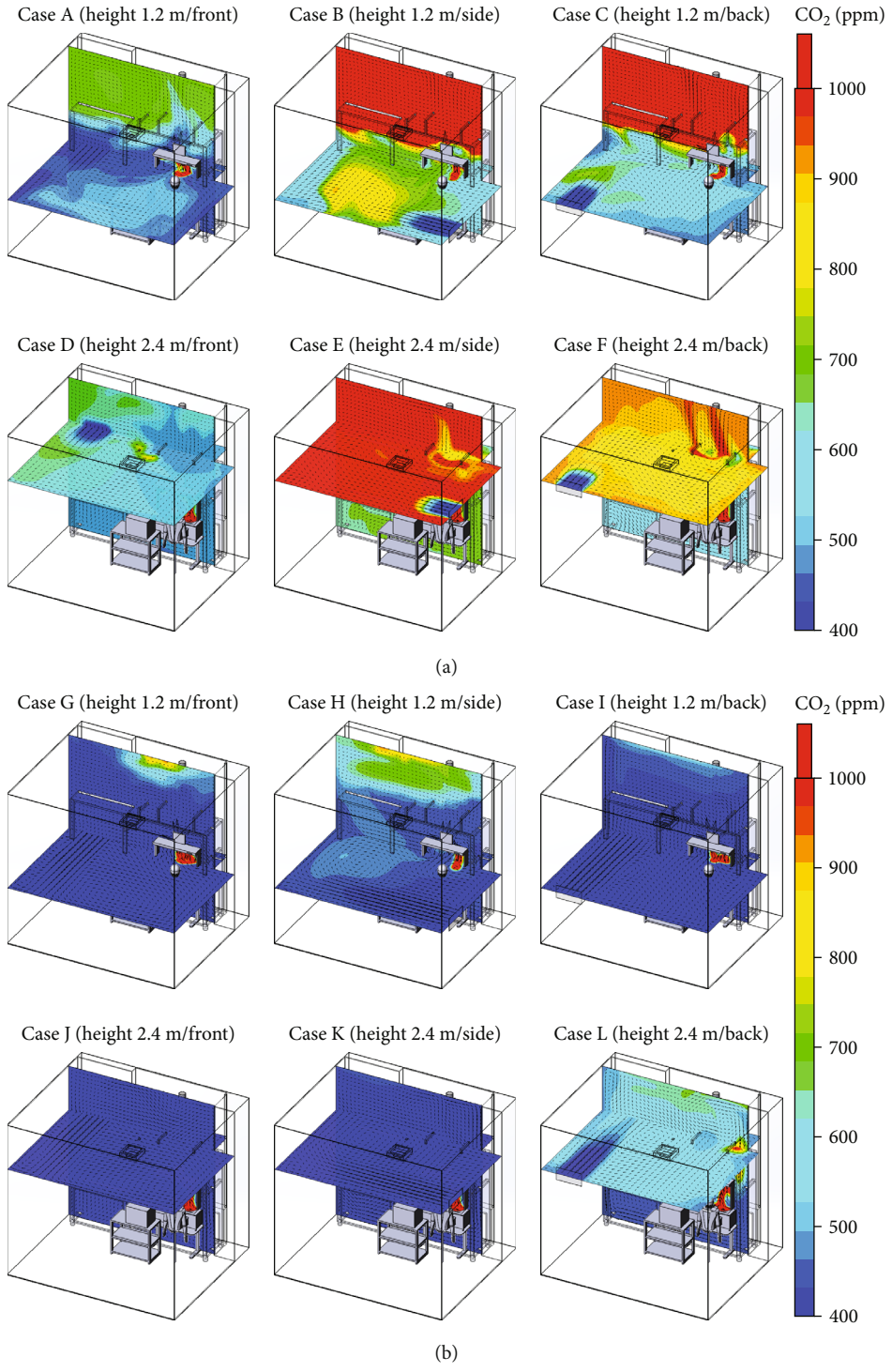

FIGURE 7: Distribution of the CO_2 concentration and the airflow velocity in the x-z plane of the window center and the x-y plane of the chamber center under the flow rate of (a) 6.72 m^3/min and (b) 12.16 m^3/min. The airflow velocity is presented using vectors, whereas the color contour describes the distribution of CO_2 concentration.

including hood design (coverage), the range of the flow rate, and burner type and position [13, 14, 22, 35, 36]. However, no experimental studies have investigated the effects of window openings on CE. Despite the differences in ventilation scenarios, CE values reported in this study were comparable to those from the laboratory and the household kitchen environment. Table 5 shows the comparison of CE for the back-burner positions from different studies under the flow rates comparable to the low flow scenarios in this study. In general, previous studies were conducted with windows closed. Their CE was overall >75%, except for the hoods from Singer et al. and was in a similar range to our findings

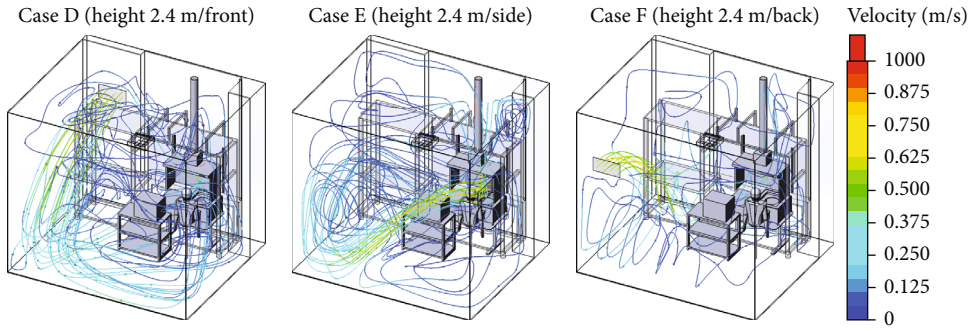

Figure 8: Distribution of the velocity flow trajectories.

Table 4: Capture efficiency (CE) of the simulation cases and the percent increase (%) in CE by exhaust flow rate and window position.

Exhaust flow rate (m^3/min)	Window height (m)	Window position		
		Front	Side	Back
CE (%)				
6.72	1.2	81 (case A)	33 (case B)	56 (case C)
	2.4	83 (case D)	49 (case E)	65 (case F)
12.16	1.2	97 (case G)	85 (case H)	97 (case I)
	2.4	97 (case J)	97 (case K)	77 (case L)
Percent increase in CE from low to high flow rate (%)	1.2	20	158	73
	2.4	17	98	18

Table 5: CO_2-based capture efficiency (CE) from previous studies with the back burner under the highest or comparable flow rate to the low flow setting (6.72 m^3/min) in our studies [13, 22, 35, 36].

Authors (year)	Study site	Ventilation status	Flow rate (m^3/min)	Range of CE (%)
Singer et al. (2012) [36]	Residence	Windows closed	6.30-7.20	45-100
Delp and Singer (2012) [22]	Laboratory	Controlled conditions with no windows	7.08*	>80
Lunden et al. (2015) [35]	Laboratory	Controlled conditions with no windows	4.80-8.28	>90
Singer et al. (2017) [13]	Residence	Windows closed; no HVAC	1.14-9.18	75 to >95
This study (2024)	Laboratory	One window with six opening positions	6.72	Front windows: 81-83 Side windows: 33-49 Back windows: 56-65

*HVI-recommended flow rate. HVAC = heating, ventilation, and air conditioning.

with the front windows open [36]. However, we found that opening the back or the side windows for ventilation could impede the hood performance considerably. This suggested that CE from previous studies might have represented better-case scenarios regarding the protective effects of exposure. Additionally, the two-burner position in the present study is more similar to the back-burner positions in other studies by providing a well-covered range to capture the thermal plume and pollutant emissions. CE for the front-burner positions was found to be lower, with a deduction of 20-25%, as reported by Singer et al. [36].

4.3. Study Strengths and Limitations. In this study, we built the simulation models based on the boundary conditions from the validation tests in the laboratory space that shared common features of a realistic, closed-type kitchen environment. One strength of the study is that we conducted four-point validation tests under steady-state conditions consistent with the assumptions of the numerical models. By having concurrent, continuous measurements at four vertical points, the validation captured the changes in temperature and CO_2 concentration gradients. Additionally, there was no interference of CO_2 from human breathing in the experimental setting. Another strength lies in practicality. It was unrealistic to install windows in all six positions for the hood performance tests in the same kitchen. Alternatively, field experiments using different kitchen spaces with designated window positions would make the comparisons particularly challenging by introducing variability in additional parameters (e.g., kitchen layout, room volume, and environmental

conditions) that could influence the simulation results. As a result, simulation using validated models could fill this gap and provide cost-effective, reliable results to characterize hood performance.

There are also limitations regarding the generalizability of our findings. First, the models should not be generalized to kitchens with distinctly different features, for example, kitchens with open space or single-sided natural ventilation in high-rise buildings. Based on our simulation, a kitchen of a smaller size with a high hood exhaust flow rate was found to have high-velocity makeup air which could disturb the thermal plume and lead to pollutant leakage into the kitchen space. As a result, simulations for open kitchens should be validated separately due to different ventilation scenarios and airflow characteristics. Second, we did not account for the effect of reentrainment of cooking emissions commonly seen in multifamily buildings, where the windows between flats were installed on the same side as the exhausted kitchen air [37]. Gao et al. simulated the upward pollutant transmission through the windows between flats of a four-floor building using CO_2 as the tracer gas [38]. The authors found that around 7.5% of the exhausted polluted air from the second floor could reenter the upper flats (third floor) due to buoyancy effects under windless weather. In this case, opening the front window, as suggested by our findings, might not be the optimal approach to reduce human exposure to cooking emissions. Nevertheless, findings from this study provide valuable information on the choice of window opening positions to minimize residents' exposure to cooking emissions for a typical closed-type kitchen in Taiwanese homes. Furthermore, the validated models could serve as a reference for future studies with more diverse kitchen layouts and environmental conditions.

5. Conclusion

We conducted four-point validation tests of the numerical models based on CO_2 concentration and temperature measurements under steady-state conditions. The validated models were subsequently used in simulations to understand the effects of six different window opening positions and two exhaust flow rates on flow fields, CO_2 concentration and temperature distributions, and CE for hood performance. We found that the CO_2 concentration could be better reduced by having windows open at the higher location. Generally, the front windows were found to be more effective with CE > 80%, followed by the back and the side windows. We also found that as the exhaust flow rate increased from 6.72 to 12.16 m^3/min, CE reached >75% for all window positions, where the most significant increase was 1.58 times for the lower side window. To sum up, changing the relative position of the window and the exhaust hood could help disperse the incoming airflow from the window, improve the kitchen's overall ventilation, and reduce pollutant concentration. Findings from this study provide important implications that when the kitchen window is positioned and used correctly, the hood performance could be well improved to protect residents from exposure to cooking emissions, even under the low exhaust flow rate.

Abbreviations

3D: Three-dimensional
CE: Capture efficiency
CFD: Computational fluid dynamics
CO_2: Carbon dioxide
HVAC: Heating, ventilation, and air conditioning
HVI: Home Ventilating Institute
IAQ: Indoor air quality
NO_2: Nitrogen dioxide
PAHs: Polycyclic aromatic hydrocarbons
PM: Particulate matter
SIMPLE: Semi-implicit method for pressure-linked equations
Temp.: Temperature
VOCs: Volatile organic compounds.

Nomenclature

ρ: Air density
u_i and u_j: Fluid velocity in x-, y-, and z-directions
t: Time
p: Pressure
τ_{ij}: Viscous shear stress tensor
τ_{ij}^R: Reynolds stress tensor
S_i: External force component in x-, y-, and z-directions
q_i: Diffusion heat flux component in x-, y-, and z-directions
ε: Turbulence dissipation rate
Q_H: Internal heat generation
H: Specific enthalpy
h: Thermal enthalpy
μ: Viscosity
δ_{ij}: Kronecker delta function
k: Turbulent kinetic energy
μ_t: Eddy viscosity.

Data Availability

The data used to support the findings of this study are available from the corresponding author upon request.

Disclosure

A preprint has previously been published (https://papers.ssrn.com/sol3/papers.cfm?abstract_id=4261535) [39].

Conflicts of Interest

The authors declare that they have no known competing financial interests or personal relationships that could have appeared to influence the work reported in this paper.

Acknowledgments

This work was supported by Taiwan National Science and Technology Council (MOST 108-2314-B-002-101-MY3)

and the Higher Education Sprout Project of National Taiwan University (NTU-111L7256).

Supplementary Materials

Supplemental Information SI-1: characteristics of the kitchen hood. SI-2: air exchange rate measurement. SI-3: specification of the instruments used in experimental measurement. SI-4: distribution of temperature by window position and hood flow rate. SI-5: additional analysis with two times the kitchen space in cases I and L. Table S1: specification of the instruments used in experimental measurement. Figure S1: front view of the kitchen exhaust hood. Figure S2: distribution of temperature in the *y-z* plane in the breathing zone. Figure S3: distribution of the CO_2 concentration in the *y-z* plane of the breathing zone. Figure S4: distribution of the CO_2 concentration with flow trajectories. *(Supplementary Materials)*

References

[1] N. E. Klepeis, W. C. Nelson, W. R. Ott et al., "The National Human Activity Pattern Survey (NHAPS): a resource for assessing exposure to environmental pollutants," *Journal of Exposure Analysis and Environmental Epidemiology*, vol. 11, no. 3, pp. 231–252, 2001.

[2] A. P. Jones, "Indoor air quality and health," *Atmospheric Environment*, vol. 33, no. 28, pp. 4535–4564, 1999.

[3] Y. J. Zhao and B. Zhao, "Emissions of air pollutants from Chinese cooking: a literature review," *Building Simulation*, vol. 11, no. 5, pp. 977–995, 2018.

[4] K. L. Abdullahi, J. M. Delgado-Saborit, and R. M. Harrison, "Emissions and indoor concentrations of particulate matter and its specific chemical components from cooking: a review," *Atmospheric Environment*, vol. 71, pp. 260–294, 2013.

[5] C. Chen, Y. J. Zhao, and B. Zhao, "Emission rates of multiple air pollutants generated from Chinese residential cooking," *Environmental Science & Technology*, vol. 52, no. 3, pp. 1081–1087, 2018.

[6] Y. C. Ko, L. S. C. Cheng, C. H. Lee et al., "Chinese food cooking and lung cancer in women nonsmokers," *American Journal of Epidemiology*, vol. 151, no. 2, pp. 140–147, 2000.

[7] K. Belanger, J. F. Gent, E. W. Triche, M. B. Bracken, and B. P. Leaderer, "Association of indoor nitrogen dioxide exposure with respiratory symptoms in children with asthma," *American Journal of Respiratory and Critical Care Medicine*, vol. 173, no. 3, pp. 297–303, 2006.

[8] Y. Hu, J. S. Ji, and B. Zhao, "Restrictions on indoor and outdoor NO_2 emissions to reduce disease burden for pediatric asthma in China: a modeling study," *Lancet Regional Health-Western Pacific*, vol. 24, article 100463, 2022.

[9] T. Y. Chen, Y. H. Fang, H. L. Chen et al., "Impact of cooking oil fume exposure and fume extractor use on lung cancer risk in non-smoking Han Chinese women," *Scientific Reports*, vol. 10, no. 1, p. 6774, 2020.

[10] Y. J. Zhao and B. Zhao, "Reducing human exposure to $PM_{2.5}$ generated while cooking typical Chinese cuisine," *Building and Environment*, vol. 168, article 106522, 2020.

[11] O. Han, A. G. Li, and R. Kosonen, "Hood performance and capture efficiency of kitchens: a review," *Building and Environment*, vol. 161, article 106221, 2019.

[12] N. A. Dobbin, L. Sun, L. Wallace et al., "The benefit of kitchen exhaust fan use after cooking - an experimental assessment," *Building and Environment*, vol. 135, pp. 286–296, 2018.

[13] B. C. Singer, R. Z. Pass, W. W. Delp, D. M. Lorenzetti, and R. L. Maddalena, "Pollutant concentrations and emission rates from natural gas cooking burners without and with range hood exhaust in nine California homes," *Building and Environment*, vol. 122, pp. 215–229, 2017.

[14] L. Sun, L. A. Wallace, N. A. Dobbin et al., "Effect of venting range hood flow rate on size-resolved ultrafine particle concentrations from gas stove cooking," *Aerosol Science and Technology*, vol. 52, no. 12, pp. 1370–1381, 2018.

[15] H. R. Zhao, W. R. Chan, S. Cohn, W. W. Delp, I. S. Walker, and B. C. Singer, "Indoor air quality in new and renovated low-income apartments with mechanical ventilation and natural gas cooking in California," *Indoor Air*, vol. 31, no. 3, pp. 717–729, 2021.

[16] D. Rim, L. Wallace, S. Nabinger, and A. Persily, "Reduction of exposure to ultrafine particles by kitchen exhaust hoods: the effects of exhaust flow rates, particle size, and burner position," *Science of the Total Environment*, vol. 432, pp. 350–356, 2012.

[17] J. Zhou and C. N. Kim, "Numerical investigation of indoor CO_2 concentration distribution in an apartment," *Indoor and Built Environment*, vol. 20, no. 1, pp. 91–100, 2011.

[18] B. Zhou, F. Chen, Z. B. Dong, and P. V. Nielsen, "Study on pollution control in residential kitchen based on the push-pull ventilation system," *Building and Environment*, vol. 107, pp. 99–112, 2016.

[19] Z. L. Chen, J. J. Xin, and P. Y. Liu, "Air quality and thermal comfort analysis of kitchen environment with CFD simulation and experimental calibration," *Building and Environment*, vol. 172, article 106691, 2020.

[20] A. E. B. Le Hocine, S. Poncet, and H. Fellouah, "CFD modeling of the CO_2 capture by range hood in a full-scale kitchen," *Building and Environment*, vol. 183, article 107168, 2020.

[21] K. W. Yi, Y. I. Kim, and G. N. Bae, "Effect of air flow rates on concurrent supply and exhaust kitchen ventilation system," *Indoor and Built Environment*, vol. 25, no. 1, pp. 180–190, 2016.

[22] W. W. Delp and B. C. Singer, "Performance assessment of U.S. residential cooking exhaust hoods," *Environmental Science & Technology*, vol. 46, no. 11, pp. 6167–6173, 2012.

[23] Y. Liu, J. K. Dong, Y. Wang, W. K. Zheng, and Y. Q. Jiang, "Numerical investigation on the influence of natural make-up air in Chinese-style residential kitchen on indoor environment in a partitioned household," *Sustainable Energy Technologies and Assessments*, vol. 46, article 101244, 2021.

[24] F. S. Xu and Z. Gao, "Transport and control of kitchen pollutants in Nanjing based on the Modelica multizone model," *Journal of Building Performance Simulation*, vol. 15, no. 1, pp. 97–111, 2022.

[25] L. Sun and L. A. Wallace, "Residential cooking and use of kitchen ventilation: the impact on exposure," *Journal of the Air & Waste Management Association*, vol. 71, no. 7, pp. 830–843, 2021.

[26] Y. B. Wang, H. X. Li, and G. H. Feng, "Numerical study of the influence of ventilation modes on the distribution and deposition of particles generated from a specific cooking process in a residential kitchen," *Indoor and Built Environment*, vol. 30, no. 10, pp. 1676–1692, 2021.

[27] L. J. He, G. Gao, J. Chen et al., "Experimental studies of natural make-up air distribution in residential kitchen," *Journal of Building Engineering*, vol. 44, article 102911, 2021.

[28] Y. J. Zhao, A. G. Li, P. F. Tao, and R. Gao, "The impact of various hood shapes, and side panel and exhaust duct arrangements, on the performance of typical Chinese style cooking hoods," *Building Simulation*, vol. 6, no. 2, pp. 139–149, 2013.

[29] W. C. Lee, P. J. Catalano, J. Y. Yoo, C. J. Park, and P. Koutrakis, "Validation and application of the mass balance model to determine the effectiveness of portable air purifiers in removing ultrafine and submicrometer particles in an apartment," *Environmental Science & Technology*, vol. 49, no. 16, pp. 9592–9599, 2015.

[30] A. Sobachkin and G. Dumnov, "Numerical basis of CAD-embedded CFD," in *NAFEMS World Congress*, Salzburg, Austria, 2014.

[31] C. K. G. Lam and K. Bremhorst, "A modified form of the k-ε model for predicting wall turbulence," *Journal of Fluids Engineering-Transactions of the Asme*, vol. 103, no. 3, pp. 456–460, 1981.

[32] S. V. Patankar, *Numerical Heat Transfer and Fluid Flow*, Hemisphere Publishing Corporation, Washington, 1980.

[33] Y. G. Li and A. Delsante, "Derivation of capture efficiency of kitchen range hoods in a confined space," *Building and Environment*, vol. 31, no. 5, pp. 461–468, 1996.

[34] J. K. Chen, R. F. Huang, and K. L. Peng, "Flow characteristics and spillage mechanisms of wall-mounted and jet-isolated range hoods subject to influence from cross draft," *Journal of Occupational and Environmental Hygiene*, vol. 9, no. 1, pp. 36–45, 2012.

[35] M. M. Lunden, W. W. Delp, and B. C. Singer, "Capture efficiency of cooking-related fine and ultrafine particles by residential exhaust hoods," *Indoor Air*, vol. 25, no. 1, pp. 45–58, 2015.

[36] B. C. Singer, W. W. Delp, P. N. Price, and M. G. Apte, "Performance of installed cooking exhaust devices," *Indoor Air*, vol. 22, no. 3, pp. 224–234, 2012.

[37] M. Kaes, N. Jajal, S. Z. Shahvari et al., "Dilution of airborne contaminants from through-wall exhausts located on the side of multi-family residential buildings," *Building and Environment*, vol. 222, article 109379, 2022.

[38] N. P. Gao, J. L. Niu, M. Perino, and P. Heiselberg, "The airborne transmission of infection between flats in high-rise residential buildings: tracer gas simulation," *Building and Environment*, vol. 43, no. 11, pp. 1805–1817, 2008.

[39] Y. A. Lin, Y. C. Chan, and W. C. Lee, "Effects of window position and exhaust flow rate on residential kitchen hood performance: a validated numerical approach," https://ssrn.com/abstract=4261535.